Journal of Building Engineering 53 (2022) 104564

Contents lists available at ScienceDirect

Journal of Building Engineering

journal homepage: www.elsevier.com/locate/jobe

Influence of mixture design parameters on the static and dynamic compressive properties of slag-based geopolymer concrete

Zhihua Ou [a,b], Ruiping Feng [a], Taiwei Mao [a], Ning Li [c,*]

[a] School of Civil Engineering, Hunan University of Technology, Zhuzhou, 412007, China
[b] Hunan Healthy City Construction Engineering Technology Research Center, Hengyang, 421001, China
[c] School of Engineering, University of Glasgow, G12 8LT, Glasgow, United Kingdom

ARTICLE INFO

Keywords:
Slag-based geopolymer concrete
Uniaxial compression
Dynamic compressive behavior
Split hopkinson pressure bar (SHPB)
Mechanical properties

ABSTRACT

This study investigated the influences of water-to-binder mass ratio (0.44, 0.47, and 0.50), and waterglass (8%, 12% and 16%) and fly ash (0%, 25% and 50%) contents on the slump, cubic compressive strength, and static and dynamic compressive behaviors of slag-based geopolymer concrete (GC). Static compressive tests were carried out by using an electro-hydraulic servo-controlled compressive test system, and dynamic ones were performed by using a split Hopkinson pressure bar (SHPB) apparatus. The specimens with a wide range of the compressive strength (from 50 MPa to 80 MPa) were prepared. The results show that the workability of fresh slag-based GC increased with increasing water-to-binder ratio, and waterglass and fly ash contents. The cubic compressive strength increased with the decreases of water-to-binder ratio and fly ash content, and the increase of the waterglass content. Increasing waterglass content contributed to the improvement of the static compressive behavior of slag-based GC, such as elastic modulus and peak stress, while it led to the rise of the brittleness. Slag-based GC with different water-to-binder mass ratios, and waterglass and fly ash contents showed a strong strain-rate dependency. However, the inclusion of 50% fly ash induced a sharp increase of the dynamic compressive strength and dynamic increase factor (DIF) at a high strain rate. Moreover, both the two formulations for fitting static compressive stress-strain curve and DIF with higher accuracy were proposed in this study.

1. Introduction

Geopolymer, as a low carbon binder, has been considered as one of the most promising alternatives to ordinary Portland cement (OPC) due to its comparable or superior mechanical property, excellent durability, better fire resistance [1–4]. It has been known that the use of geopolymer to manufacture corresponding concrete could potentially solve the solid waste disposing problems, such as land occupation by stocking and landfilling [5] and further decrease the natural resource and energy consumptions during the construction process [6,7].

However, the existing research concentrated on exploring the reaction mechanism at the micro-level cannot fully support the future application in geopolymers, particularly involved in the mechanical responses [8,9]. This is because of lacking of standardization of geopolymer concrete (GC) due to the inconsistency of raw materials and the complexity of mixture designs with more variable parameters of GC [10]. Understanding the mechanical response of GC is essential as well, which can contribute to the application of GC.

* Corresponding author.
E-mail address: Ning.Li@glasgow.ac.uk (N. Li).

https://doi.org/10.1016/j.jobe.2022.104564
Received 24 November 2021; Received in revised form 3 April 2022; Accepted 23 April 2022
Available online 26 April 2022

However, due to the higher brittleness of geopolymer than that of OPC [11,12], there is a resultant difference of mechanical response between the both. Ding et al. [1] comprehensively reviewed the static and dynamic mechanical performances of GC with different binder compositions and concluded that there was an inadaptability of using the current constitutive model to estimate the uniaxial compressive behavior of GC. Also, extensive research reported that the GC with similar compressive strength has lower elasticity modulus than that of OPC-based concrete [13–15]. Cong et al. [8] reported that slag-based GC had a higher Poisson's ratio than OPC-based concrete. Also, GC exhibits a different dynamic response from OPC-based concrete. It was reported that slag/fly ash-based GC had a higher strain rate sensitivity than OPC-based concrete [16]. Gao et al. [9] found that slag-based GC had a better post-peak energy absorption capacity under impact. Recently, Liu et al. [14], and Karimipour and de Brito [17] successfully utilized geopolymer to manufacture ultra-high performance geopolymer concrete (UHPGC) and also reported that the existing mechanical performance correlations of OPC-based concrete could not be suitable for GC.

Although there has been literature published on the engineering property of GC, as mentioned above, the understanding of it is still not sufficient yet. Compared with OPC-based concrete, binder types and compositions [14,18,19], water-to-binder mass ratios, and activator type, composition and dosage [20,21], these parameters, dominantly impact the engineering performance of GC. The incorporation of slag would significantly improve the mechanical properties, while results in the reduction of workability [22]. Tang et al. [23] found that incorporations of slag in GC resulted in a sharp rising slope and steeper descending part, indicating higher brittleness of slag/fly ash-based GC. Carvalho et al. [24] reported that the increases of the activator modulus and alkali content (Na_2O %) would improve the compressive and flexural strengths of municipal solid waste incineration bottom ash-based geopolymer. Ding et al. [18] reported that the increase of the SiO_2/Na_2O molar ratio of the activator from 1.0 to 2.0 improved the ductility of slag-based GC. Also, Xin et al. [16] conducted the split Hopkinson pressure bar (SHPB) test on slag/fly ash-based GC with different activators and found that the dynamic compressive deformation behavior of GC with sodium hydroxide and silicate blended activator was better. On the other hand, the Si from activator and binders would change the microstructure and resultant mechanical performance such as Young's modulus by changing the Si/Al ratio of the system [25]. Thus, it is of great necessity of evaluating the influence of those mixture parameters on the engineering property of GC.

Based on the above, the purpose of this investigation is to explore the influence of water-to-binder mass ratio (0.44, 0.47 and 0.50), waterglass (8%, 12% and 16%) and fly ash contents (0%, 25% and 50%) on the engineering property of slag-based GC including workability, compressive strengths of the cubic and prismatic specimens, uniaxial compressive behavior, and dynamic response. Furthermore, the constitutive model of slag-based GC under uniaxial compression was proposed, and the relation between the dynamic increase factor (DIF) and strain rate for the specimens with high waterglass and fly ash amount was established. Finally, the understanding on the influence of those factors on the static and dynamic mechanical performance of slag-based GC can be deepened based on this study.

2. Experimental programs

2.1. Raw materials

Slag and fly ash were employed as binders in this research. Table 1 shows their chemical composition determined by X-ray fluorescence. An industrial graded sodium hydroxide (SH) with a purity of 99% was used. The parameters of liquid sodium silicate (LSS) used in this study, were: 56.7 wt% H_2O, 32.99 wt% SiO_2 and 10.31 wt% Na_2O. The waterglass was prepared with blending SH and LSS and its SiO_2/Na_2O ratio was adjusted to 1.0. The granite aggregate with a maximum size of 13.2 mm and river sand with a fineness of 2.80 were used in this study. The aggregates were dried before preparing GC. The grading curves of granite and sand aggregates are shown in Fig. 1. Tap water was used to prepare GC mixtures.

2.2. Mix proportions and specimen preparation

The mixture proportions of slag-based GC are presented in Table 2. Three water-to-binder mass ratios (0.44, 0.47, 0.50) were adopted to study the effect of water-to-binder mass ratio on the slump and mechanical performance of slag-based GC. Here water includes additional water and water from the waterglass, and the binder contains dried precursor powders and the solid content in waterglass. Also, to investigate the influence of waterglass content, waterglass was mixed in three mass percentages (8%, 12% and 16%) under a constant water-to-binder mass ratio of 0.47. In addition, three mixtures with different fly ash contents (0, 25% and 50%) and a content water-to-binder mass ratio of 0.47 were prepared to investigate the influence of fly ash content on the slump and mechanical performance of slag-based GC.

The waterglass was prepared 1 day prior to concrete casting. The coarse and fine aggregates were added into the mixer and mixed for not less than 3 min. Then, tap water and waterglass were added and stirred for 5 min. Fresh concrete mixtures were cast in the molds and compacted on a vibration table. Afterwards, the samples with the molds were first pre-cured for 24 h at a curing room with a constant temperature of 20 °C and a relative humidity higher than 95%. Plastic films were used to cover the molds to avoid the penetration of water. After that, the samples were demolded and cured at the curing room with the same curing conditions until for the

Table 1
Chemical composition of slag and fly ash (wt.%).

	CaO	Al_2O_3	SiO_2	MgO	SO_3	K_2O	TiO_2	MnO	Fe_2O_3	Na_2O	P_2O_5	LOI
Slag	38.81	14.78	33.81	7.09	2.49	0.44	1.23	0.41	0.36	0.26	0.06	1.40
Fly ash	1.32	34.11	52.64	0.50	0.33	1.38	1.72	0.02	3.25	0.03	0.17	3.25

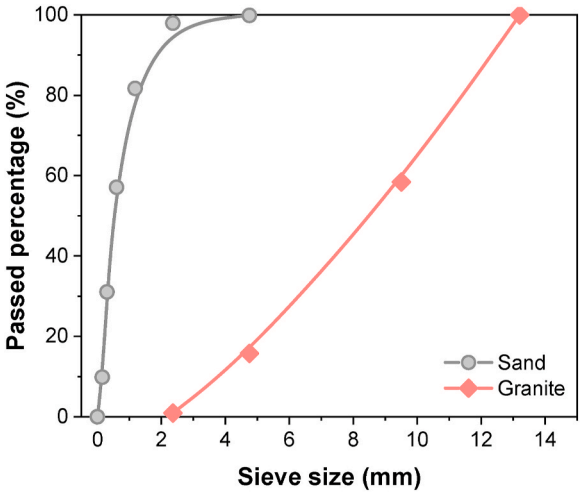

Fig. 1. Grading curves for granite and sand.

Table 2
Mixture proportions of slag-based GC.

No.	Water-to-binder mass ratio	Waterglass content (%)	Fly ash content (%)	Slag (kg/m^3)	Fly ash (kg/m^3)	Waterglass (kg/m^3)	Water (kg/m^3)	Sand (kg/m^3)	Granite (kg/m^3)
W44F0B	0.44	12	0	357	0	99	120	681	1111
W47F0B	0.47	12	0	357	0	99	132	681	1111
W50F0B	0.50	12	0	357	0	99	144	676	1104
W47F0A	0.47	8	0	370	0	68	149	681	1111
W47F0C	0.47	16	0	345	0	127	118	681	1111
W47F25B	0.47	12	25	268	89	99	132	681	1111
W47F50B	0.47	12	50	179	179	99	132	681	1111

next 27 days.

2.3. Test methods

2.3.1. Workability

The workability of fresh slag-based GC mixture was measured by slump test based on the China's national standard GB/T 50,080-2016 [26] (similar to Australian standard AS 1012.3.1 [27]). The slump test was carried out immediately after mixing at laboratory conditions.

2.3.2. Cubic compressive strength

The compressive strength of cubic sample of slag-based GC cured for 28 d was determined by using 200 t compression machine. The dimension of the cubic specimen was 100 mm × 100 mm × 100 mm and the loading rate was 0.5 kN/s, in accordance with China's national standard GB/T 50,081-2016 [28]. The average value of six measurements was reported.

2.3.3. Uniaxial compressive behavior

The prismatic specimens cured for 28 d with a dimension 100 mm × 100 mm × 300 mm were used. The test was performed by using an electro-hydraulic servo-controlled compressive test system (INSTRON1346). Two linear variable differential transducers (LVDT) were mounted at the middle height on the specimens for measuring the axial deformation with a gauge length of 150 mm. The compressive stress-strain behavior was recorded by combining data of the two LVDTs.

There were three stages for the loading process. The first loading process was pre-loading stage, and the specimen was subjected to 10% of the average compressive strength of the corresponding cubic specimen to avoid the slackness of the system and eccentricity of loading. Then, the load was increased to 75% of the average compressive strength of the corresponding cubic specimen with a loading rate of 0.5 kN/s. Finally, to acquire a stable descending curve of slag-based GC under compression, the loading regime was shifted to a displacement control of 0.02 mm/min. The test was continued until the load decreased to less than 1 kN or failure.

2.3.4. Dynamic compression test

The dynamic compression tests were conducted by using the 100-mm split Hopkinson pressure bar (SHPB) apparatus. The SHPB apparatus consists of a 6000-mm long input bar, a 4000-mm long output bar and a 1500-mm long strike bar, respectively. Cylinder samples cured for 28 d with a diameter of 82 mm and a height of 41 mm was used in SHPB test. The ends of each sample were ground

for making them parallel in order to ensure the reliability of the tests. Then, the samples were placed between the ends of the input and output bars. Stress waves are generated and propagated through the rod to the sample at the end of the input rod. This incident wave splits into transmitted and reflected waves upon arrival at the sample. The transmitted wave passes through the sample and enters the output bar, inducing the plastic deformation of the sample. The reflected wave was reflected away from the sample and response to the input bar. The whole process is automatically recorded by the computer.

2.3.5. Scanning electron microscopy (SEM) analysis

The crushed samples were extracted for microscopic testing. SEM observation was conducted by using Phenom Pro X. An accelerating voltage of 5 kV and working distance of 10 mm were used to obtain the better spatial resolution.

3. Results and discussion

3.1. Slump

The influences of water-to-binder mass ratio, waterglass and fly ash contents on the slump of slag-based GC are shown in Fig. 2. It can be seen that the slumps of the fresh slag-based GC mixtures increase with the increases of water-to-binder mass ratio, waterglass and fly ash contents, which is consistent with the previous study [22]. When the water-to-binder mass ratio increases from 0.44 to 0.47, the slump of the fresh mixture almost linearly increases from 163 mm to 230 mm. Also, as the waterglass content increases from 8% to 16%, the slump of the fresh mixture increases from 122 mm to 203 mm. However, the positive effect of waterglass content on the slump becomes less considerable when the waterglass content exceeds 12%. It should be noted that in this research, the modulus of the waterglass used is constant, that is to say, the increase of waterglass content mainly influences the Na_2O-to-binder mass ratio and the concentration of sodium silicate of the system. Therefore, given the waterglass used in this paper, with a satisfied modulus of 1.0 [29], increasing waterglass content would not only lead to the increase of alkali content, but also the silicate concentration, which would contribute to the dispersion of particles, thus improving the workability [30]. On the other hand, once the waterglass content further increases (>12%), the excessive alkali ions would induce an increase in yield stress induced by the attractiveness of the electric double layer [31], thus receding the positive influence of increasing waterglass content on the slump. Furthermore, given a constant water-to-binder mass ratio, increasing fly ash content from 0% to 50% leads to the increase of the slump from 195 mm to 218 mm. This is attributed to the lubricating and ball-bearing effects of fly ash, as reported in the previous research [22,32,33].

3.2. Cubic compressive strength

Fig. 3 shows the influences of water-to-binder mass ratio, waterglass and fly ash contents on the cubic compressive strength of slag-based GC cured for 28 d. It can be seen that the increases of water-to-binder mass ratio and fly ash content both play a negative role in

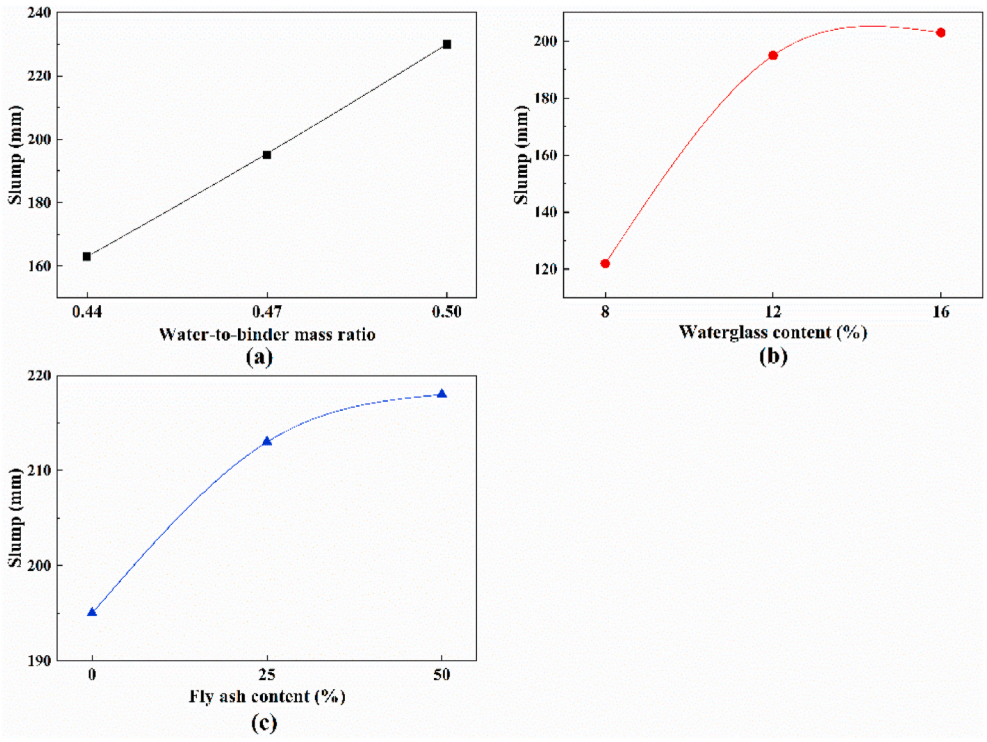

Fig. 2. Influences of (a) water-to-binder mass ratio, (b) waterglass content, and (c) fly ash content on the slump of slag-based GC.

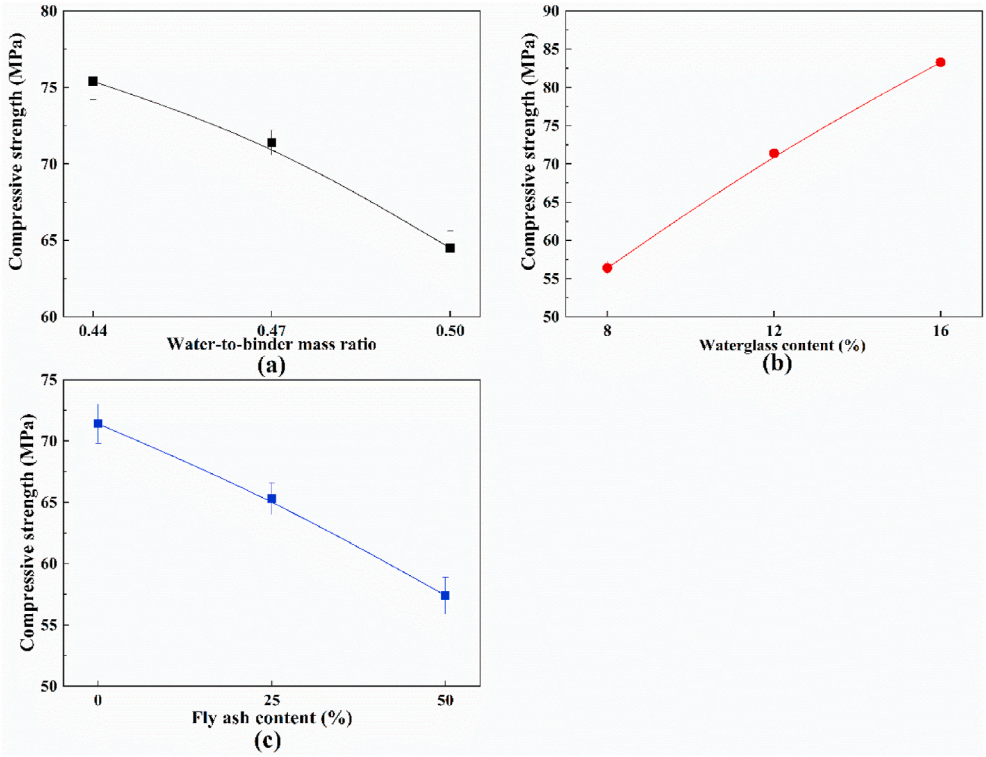

Fig. 3. Influences of (a) water-to-binder mass ratio, (b) waterglass content, and (c) fly ash content on the cubic compressive of slag-based GC.

the compressive strength, while the compressive strength improves as the waterglass content increases. The compressive strength of the sample decreases from 75.4 MPa to 64.5 MPa when the water-to-binder mass ratio increases from 0.44 to 0.50. This is consistent with the previous research [18,22]. More addition of water into the mixture would result in the increment of the water evaporation from the pore, which consequently increases the porosity [34].

On the other hand, the compressive strength of the cubic specimens increases from 56.4 MPa to 83.3 MPa with the increase of waterglass content from 8% to 16%. This is consistent with the previous literature [18,34]. The Na_2O-to-binder mass (N/B) ratios of the samples with 8%, 12% and 16% waterglass content are approximately 3.2%, 5.9% and 7.9%, respectively. According to Li et al. [22], the compressive strength is strongly dependent upon the N/B ratio, given a constant water-to-binder mass ratio. Furthermore, the compressive strength decreased from 71.4 MPa to 57.4 MPa when the fly ash content increases from 0% to 50%. Compared to slag, fly ash has less reactivity, thus reducing the compressive strength [35].

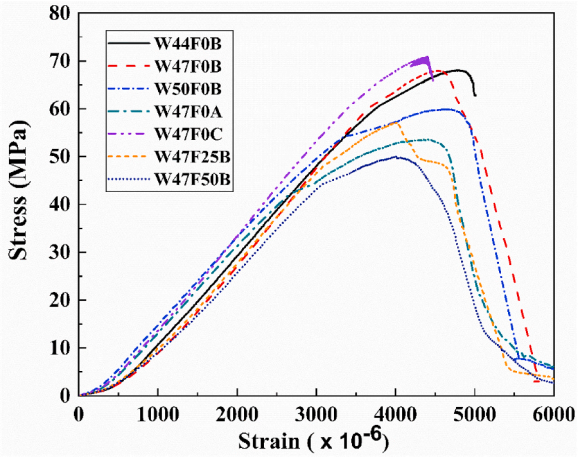

Fig. 4. Compressive stress-strain curves of slag-based GC with different water-to-binder mass ratios, waterglass contents and fly ash contents.

3.3. Static uniaxial compression behavior

3.3.1. Stress-strain behavior

As mentioned in Section 2.3.3, the axial strain of each specimen was obtained by calculating the mean value of two LVDTs. The axial stress was calculated by dividing the loads by the cross-sectional area of the prismatic specimen. The stress-strain curves of slag-based GC with different water-to-binder ratios, waterglass and fly ash contents are shown in Fig. 4. Similar to the previous research concentrated on the uniaxial compressive behavior of GC by Tang et al. [23] and Zhang et al. [36], the stress-strain curve of slag-based GC consists of two parts, which are ascending stage and descending stage, respectively. Moreover, the initial part of the ascending portion of the stress-strain curve is linear, while a slow increase of the stress is observed when the stress increases to about 80% peak stress. Furthermore, water-to-binder-mass ratio, waterglass and fly ash contents have a significant influence on the static compressive behavior at the post-peak stage. It can be seen that the specimens with a lower water-to-binder mass ratio, higher waterglass and lower fly ash contents cannot present higher peak stress, greater slope at the ascending portion, while have a stress-strain curve with a full descending part. This corresponds to the results in Section 3.2; that is to say, the specimens with higher compressive strength exhibit a higher brittleness, as reported in the previous research [18,23,37].

Table 3 lists the average values and the corresponding coefficients of variation of the modulus of elasticity, peak stress and strain (the stress and the corresponding strain at the peak point), residue stress and ultimate strain (the stress and the corresponding strain at the inflection point of the descending portion), toughness (area under the stress-strain curves up to the peak point) of the stress-strain curves. The modulus of elasticity was based on the slope of the curve at the ascending part of the curve from the stress of 5 MPa to the stress of 40% peak stress [14].

From Table 3, it can be found that the increase of water-to-binder mass ratio from 0.44 to 0.50 leads to the reductions of the elastic modulus and peak stress of the specimens from 19.1 GPa to 16.5 GPa, and 69.4 MPa–56.7 MPa, respectively. This could be attributed to the increased porosity of the specimens when more water is added, as discussed in Section 3.2. Moreover, the peak stress and strain are improved when the waterglass content increase from 8% to 12%. However, it can be found that waterglass content has a considerable influence on the elastic modulus and toughness. In addition, the specimens with higher waterglass content (>8%) exhibit higher brittleness, which results in the absences of the residual stress and ultimate stress. The inclusion of fly ash induces the degradation of the uniaxial compressive performance of slag-based GC, which is consistent with the previous studies [1,8]. This is because that the incorporation of fly ash would contribute to the formation of N-A-S-H gel, which has a lower Young's modulus than C-A-S-H gel, the main reaction product in the activation of slag [25,38]. In addition, increasing fly ash content would weaken the interfacial transition zones between aggregate and binder [23].

3.3.2. Establishment of the constitute model for slag-based GC under uniaxial compression

Tang et al. [23] proposed a model for slag/fly ash-based GC with high accuracy by modifying the one developed by Collins et al. [39], which is described as:

For the ascending part:

$$y = x\frac{A}{A-1+x^{A}} \quad 0 \le x \le 1 \tag{1}$$

For the descending part:

$$y = x\frac{A}{A-1+x^{AB}} \quad 1 \le x \tag{2}$$

Also, a good correlation between the parameters and peak stress of the specimens in the proposed model by Tang et al. [23] is found, demonstrating a specific physical meaning. Guo et al. [40] proposed a model for OPC-based concrete under compression, which has been extensively used and is described as:

For the ascending part:

$$y = Ax + (3-2A)x^{2} + (A-2)x^{3} \quad 0 \le x \le 1 \tag{3}$$

For the descending part:

Table 3
Stress-strain characteristics of slag-based GC.

No.	Elastic modulus (GPa)/CoV (%)	Peak stress (MPa)/ CoV(%)	Peak strain (× 10^{-6})/CoV (%)	Residual stress (MPa)/CoV(%)	Ultimate strain (× 10^{-6})/CoV (%)	Toughness (MPa)/ CoV(%)
W44F0B	19.1/5.06	69.4/1.94	4696/2.98	-	-	0.179/3.57
W47F0B	17.4/3.98	67.2/1.99	4480/0.58	-	-	0.148/4.36
W50F0B	16.5/9.34	56.7/9.45	4682/0.88	42.1/2.13[a]	5133/1.27[a]	0.162/6.35
W47F0A	15.4/1.46	53.3/0.36	4227/6.85	38.7/0.99[a]	4622/5.46[a]	0.144/11.84
W47F0C	18.0/4.76	65.8/6.85	4337/9.07	-	-	0.142/17.06
W47F25B	15.3/7.28	56.7/9.48	4115/7.67	51.3/10.25	4307/8.29	0.111/10.67
W47F50B	15.3/1.71	49.4/0.95	3956/0.81	42.7/4.33	4444/0.95	0.101/0.51

[a] Data calculated based on two experimental curves due to missing descending segment in one of the experiments.

$$y = \frac{x}{B(x-1)^2 + x} \quad 1 \le x. \tag{4}$$

Fig. 5 illustrates the fitting results of the above-mentioned model and average stress-strain curves after normalization of the specimens. The fitting outcomes of the proposed model by Tang et al. [23] are closer to the experimental curves, than that by Guo et al. [40]. Furthermore, it can be found that for the normalized stress-strain curves without a complete descending portion, the two models both exhibit a high determination coefficient (R^2). As shown in Fig. 5 (a) and (b), the determination coefficients of those both exceed 0.95, indicating high fitting accuracy on the ascending part. Nevertheless, the underestimation on the descending part of the experimental curves leads to a high fitting error, which generates some discrepancies between the fitting outcomes of these models and experimental stress-strain curves having a full descending branch, except that of the specimen W47F50B. This could be mainly attributed to (a) a large compressive strength span among the specimens for fitting based on the existing models, and (b) variations of the mixture design parameters as discussed in Section 3.2. On the other hand, from Fig. 5, it can be found that a steeper curve at the descending part for the fitting curves based on the model proposed by Guo et al. [40]. To sum up, the existing models for the descending branch of the stress-strain curve of slag-based GC should be further modified.

Therefore, based on the above discussion and the compressive behavior of slag-based GC, a stress-strain model is proposed in this paper, which can be expressed as:

For the ascending part:

$$y = Ax + (3-2A)x^2 + (A-2)x^3 \quad 0 \le x \le 1 \tag{5}$$

For the descending part:

$$y = x\frac{B}{B-1+x^B} \quad 0 \le x \le 1 \tag{6}$$

This proposed model is established by combing the models developed by Guo et al. [40], Tang et al. [23] and Collins et al. [39]. Adopting Eq. (3) from the model of Guo et al. [40] as the model for the ascending part of the stress-strain curve of slag-based GC is based on a comparative analysis. On the other hand, as discussed before, there is an underestimation of the fitting curve at the descending branch. Therefore, in order to remedy this, Eq. (1), rather than Eq. (2), is adopted for fitting the descending part of the stress-strain curve of slag-based GC. Fig. 6 depicts the fitting results of the proposed models in this study. The parameters and determination coefficients of the fitted outcomes are given in Fig. 6 as well. It can be found that the fitted curves based on the model proposed in this study fit well with the normalized experimental ones. Also, a higher determination coefficient above 0.95 of the fitted curves is acquired, indicating the high accuracy of this model. On the other hand, the values of the parameters A and B of the model are influenced by the changes of the water-to-binder mass ratio, waterglass and fly ash contents. This implies that the parameters probably have physical meanings, which requires further confirmation and investigation.

3.4. Dynamic compression

3.4.1. Stress equilibrium

The typical pulses monitored from the strain gauges during the SHPB test including the incident pulse, transmitted pulse and

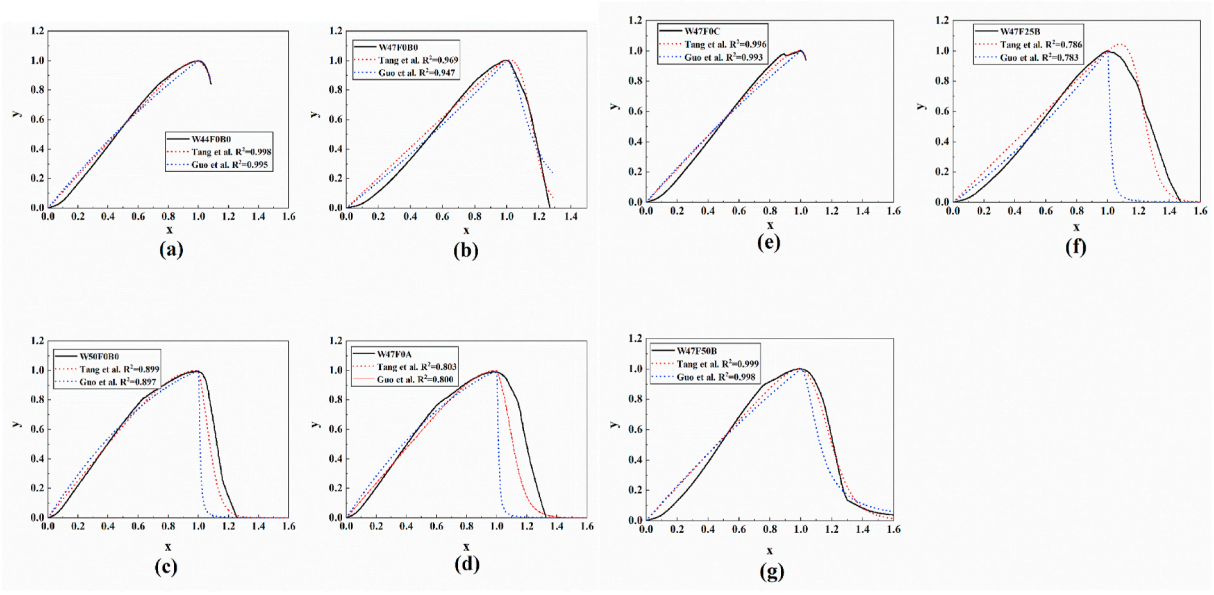

Fig. 5. Comparison between the fitting results based on the existing models [23,40] and normalized experimental curves.

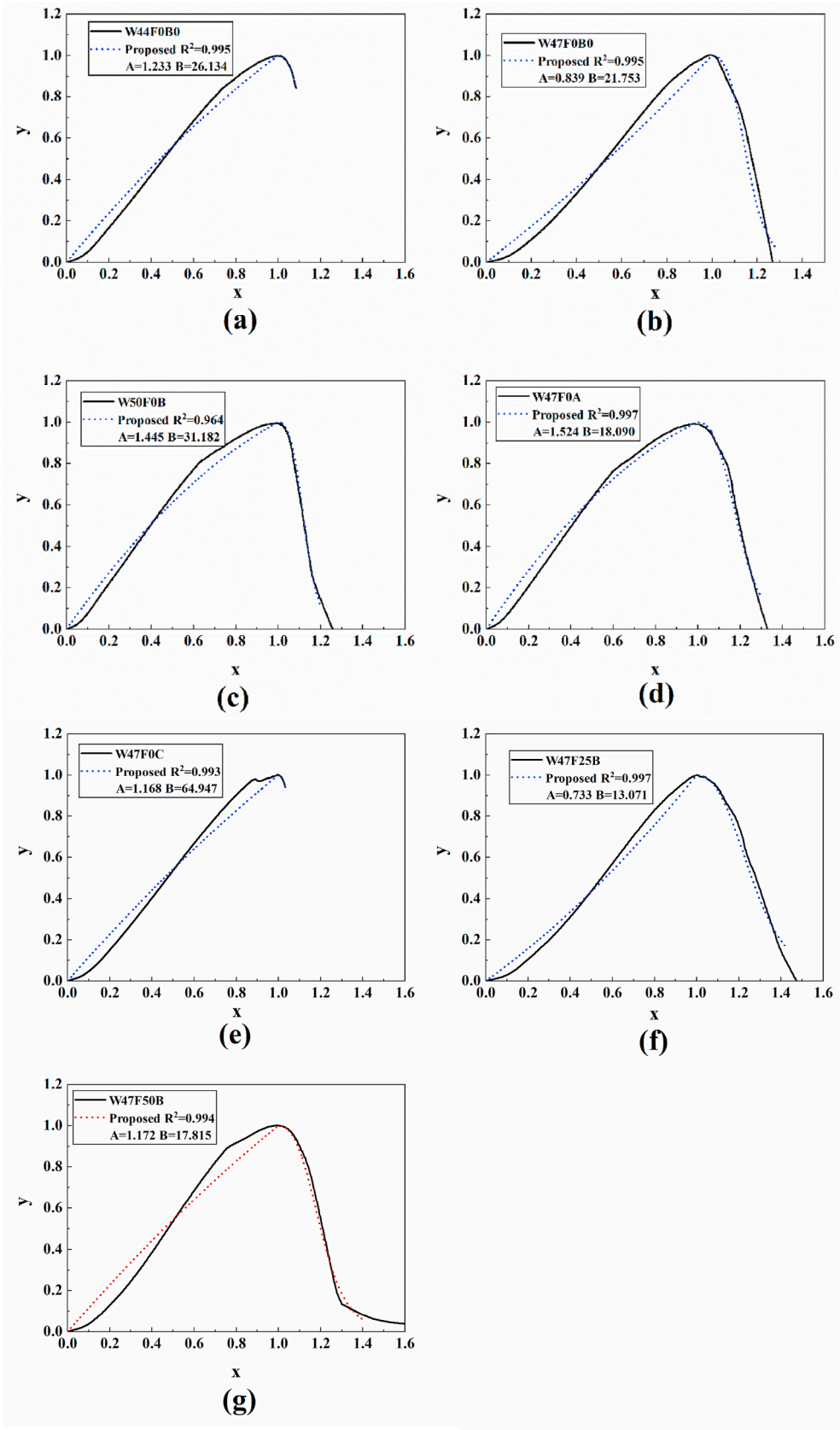

(caption on next page)

Fig. 6. Comparison between the proposed stress-strain model and normalized experimental curves of slag-based GC.

reflected pulse, are shown in Fig. 7. Based on the theory of one-dimensional stress wave, the stress ($\sigma s(t)$), strain ($\varepsilon s(t)$), and strain rate ($\dot{\varepsilon}_s(t)$) can be obtained through the conversion of the measurement data, which can be expressed, respectively, as [41,42]:

$$\sigma_s(t) = \frac{E_0 A_0}{A_S}\varepsilon_t(t) \tag{7}$$

$$\varepsilon_s(t) = \int_0^t \dot{\varepsilon}_s(\tau)d\tau \tag{8}$$

$$\dot{\varepsilon}_s(t) = \frac{2C_0}{L_s}\varepsilon_R(t) \tag{9}$$

in which, A_0, E_0, and C_0 are the cross-sectional area, the modulus of elasticity, and the velocity of the elastic wave, of the SHPB bars, respectively; A_s and L_s are the cross-sectional area and height of the samples, respectively; ε_R (t) and $\varepsilon_t(t)$ refer to the reflected strain and the transmitted strain, respectively. The data processing and stress equilibrium were examined to ensure the validity of the SHPB tests based on the previous research [43,44]. The typical signal after the removal of time lags is presented in Fig. 8 (a). It was observed that ε_I $(t) + \varepsilon_R$ (t) is consistent with ε_T (t), indicating the achievement of stress equilibrium. The stress in the specimen was considered approximately uniform only when the quotient of the difference between the forces at the two ends of specimen to the average value (R) is less than 0.05 [45]. The variation of R with time is presented in Fig. 8 (b). During the dynamic loading period (i.e., between 50 μs and 100 μs), R remains below 0.05, implying that the dynamic force balance is reached in the compression specimen. Therefore, the force equilibrium state is achieved during the most dynamic compression loading period. The test that satisfied this stress equilibrium conditions was considered valid.

3.4.2. *Dynamic stress-strain curve*

Fig. 9 depicts the dynamic stress-strain curves of slag-based GC with different water-to-binder mass ratios, waterglass and fly ash contents under different strain rates. The peak stress in the dynamic compressive stress-strain curve is typically higher compared to that of uniaxial compressive stress-strain curve. This is consistent with the previous studies [9,44,46]. There is a sensitivity of the peak stress of the dynamic stress-strain curve to the strain rate, that higher strain rate leads to a higher peak stress among the specimens. This dependence could be attributed to the Stefan effect, the effect of cracking propagation, and the inertia-induced lateral confinement effect [44].

The influences of water-to-binder mass ratio, waterglass and fly ash contents on the dynamic compressive stress-strain behavior are different from those on the uniaxial compressive curve. It can be found that at a similar grade of strain rate, the peak stress decreases with the increase of water-to-binder mass ratio, and the decrease of waterglass content. However, interestingly, it is obvious that the specimens with 50% fly ash possess a superior dynamic compressive stress at different levels of the strain rate and exhibits a different strain rate sensitivity from the specimen without fly ash. Moreover, when the strain rate exceeds 225 s^{-1}, the stress significantly increases for the specimens with 50%. On the other hand, incorporating fly ash results in a considerable difference in the descending part of the dynamic compressive stress-strain curve, compared with the specimen without fly ash. A steeper descending branch at the stress-strain curve of the specimen with 50% is observed. This phenomenon could be attributed to the formation of reaction products (N-A-S-

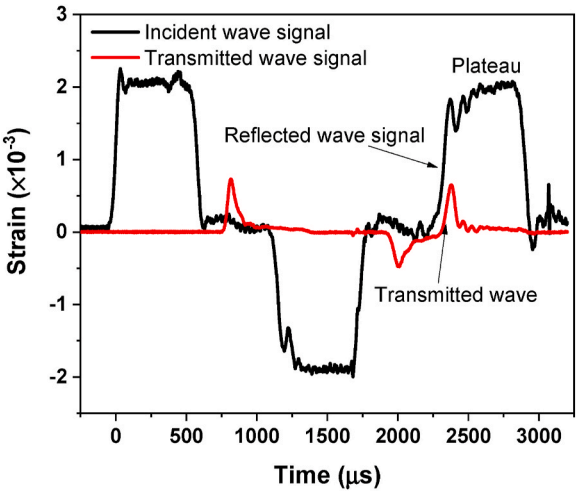

Fig. 7. Typical impact pulses of SHPB test for slag-based GC.

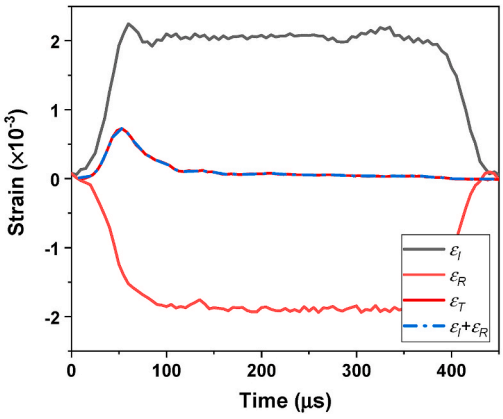

(a) Typical signal after the removal of time lags.

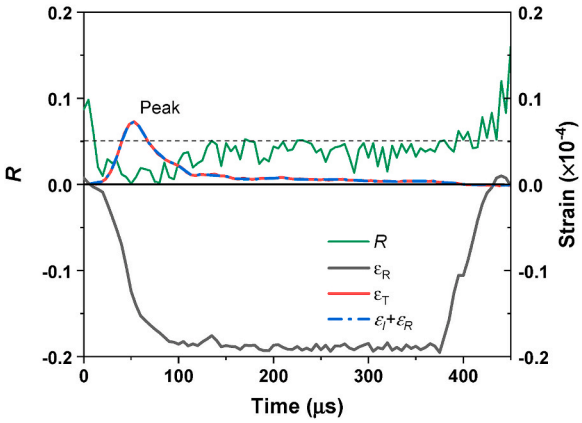

(b) Stress uniformity in the specimen

Fig. 8. Typical dynamic stress equilibrium relationship between stress and time.

H gel) with a three-dimensional structure induced by adding fly ash, thus changing the brittleness and strain sensitivity of the specimens [1].

The influence of the waterglass content on the dynamic stress-strain curve is similar to that of fly ash. As the waterglass content increases, the dynamic response increase, and it is noted that with adding 16% waterglass, the specimen exhibits a higher strain rate sensitivity and a much steeper descending part when the strain stress is at a high level of the strain rate (>275 s^{-1}), which is consistent with the previous research [47]. This could be attributed to that a higher amount of the waterglass contributes to the formation of reaction products with denser microstructure and results in a higher brittleness [18].

3.4.3. Dynamic compressive strength and dynamic increase factor

Fig. 10 shows the relationship between the dynamic compressive strength and the strain rate. The dynamic compressive strength of slag-based GC has a linear dependency on the strain rate, and it increases with the increase of strain rate; Moreover, the specimens with a higher quasi-static compressive strength presents a higher dynamic compressive response as well, which is consistent with the previous research [44,48]. Also, in Fig. 10, as the strain rate increases, the dynamic compressive strengths of the specimens W47F0C and W47F50B increase more significantly. This indicates the domination of the influence of waterglass and fly ash on the strain rate sensitivity of slag-based GC.

The dynamic increase factor (DIF) is the ratio of the dynamic compressive strength to quasi-static compressive strength, which is usually used for characterizing the strain-rate sensitivity of concrete. Fig. 11 shows the relationship between strain rate and DIF of slag-based GC and the comparison between the experimental results and the existing models for predicting DIF from the study of Tang et al. [44] and proposed by the CEB 1990 [49]. The two models are expressed as, respectively:

The model developed by Tang et al. [44]:

$$DIF = A \cdot \log\left(\frac{x}{B}\right) + 1 \tag{10}$$

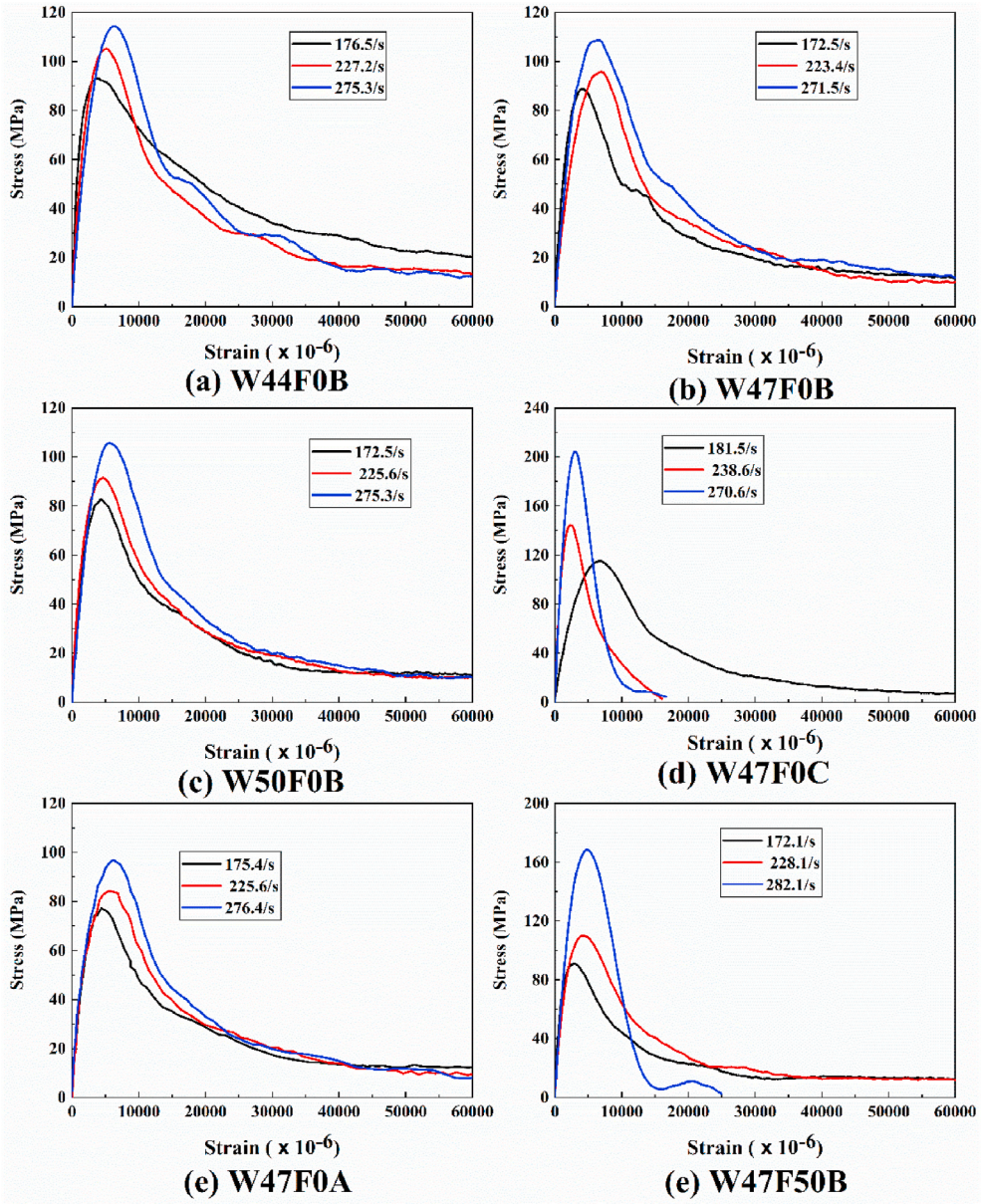

Fig. 9. Dynamic compressive stress-strain curves of slag-based GC with different water-to-binder mass ratios, and waterglass and fly ash contents under different strain rates.

The model suggested by CEB 1990 [49]:

$$DIF = 0.012\left(\frac{x}{A}\right)^{\frac{1}{3}} \quad x > 30\ s^{-1} \tag{11}$$

From Fig. 11, It can be found that the DIFs of the specimens with different water-to-binder mass ratios, and waterglass and fly ash contents increase with the increased strain rate. Also, it is noted that the specimens with 16% waterglass and 50% fly ash contents have higher DIFs, which is consistent with the previous study by Tang et al. [44]. For instance, the DIFs of the specimens with 50% fly ash content are about 1.6 when the strain rate is about 175 s^{-1}. On the other hand, the DIFs of the specimens with 50% fly ash and 16% waterglass increase sharply, and those models cannot fit well the DIFs of slag-based GC in this study, and they underestimate the DIF due to the presence of the specimens (W47F50B and W47F0C) with a dramatic strain-rate sensitivity at higher strain rate level, when the strain rate exceeds about 225 s^{-1}. In addition, it can be observed that all specimens, except W47F0B and W47F0C, show a gentle increasing trend with the increase of the strain rate, implying the feasibility of using the existing model for predicting the DIF. Therefore, it is necessary to propose a model suitable for the prediction of DIF of slag-based GC with high strain-rate dependency.

Due to a sharply-increasing trend of the DIF versus the strain rate of the specimens with 50% fly ash and 16% waterglass,

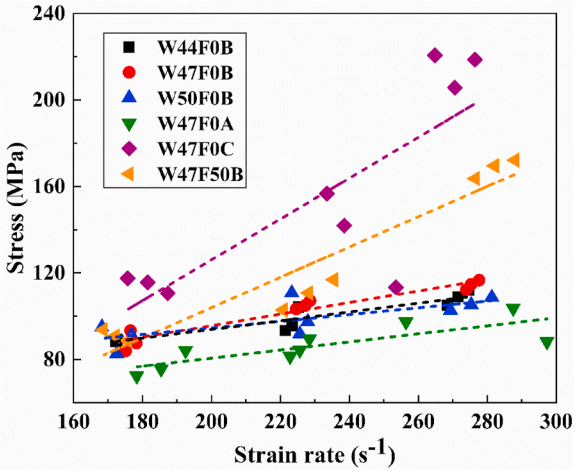

Fig. 10. Relationship between the dynamic compressive strength and strain rate for slag-based GC.

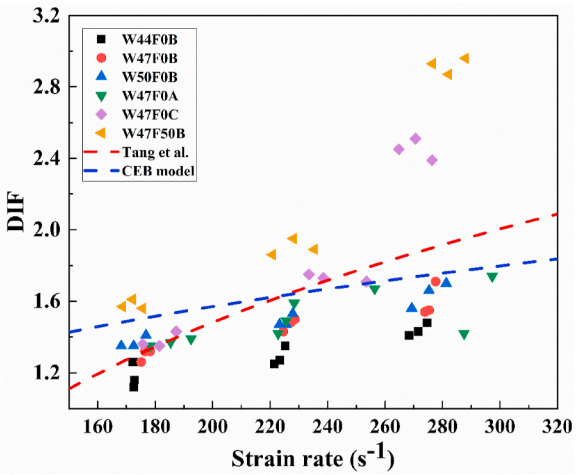

Fig. 11. Relationship between the DIF and strain rate for slag-based GC.

particularly when the strain rate exceeds 225 s^{-1}, the DIF model based on a power function is proposed in this study, which can be expressed as:

$$DIF = A \cdot x^6 + 1.4 \tag{12}$$

Fig. 12 depicts the fitted outcomes of the proposed model for the specimens of W47F50B and W47F0C and fitted results of the model proposed by Tang et al. [44]. The parameters of the fitting results are shown in Table 4. It is observed that in terms of the specimens of W47F0C and W47F50B, the model proposed in this study can predict better than that by Tang et al. [44]. On the other hand, the model proposed by Tang et al. [44] is still suitable for predicting the DIFs at higher rate level of the specimens in this study, except that of the specimens with 50% fly ash and 16% waterglass, indicating a good universality of their model for predicting DIFs of GC. Therefore, based on the above, there would be a possibility of using the model proposed herein as the complement of the DIF prediction for slag-based GC. The proposed model in this study for DIF prediction could be more suitable for the specimens with a higher DIF at a relatively low strain-rate level.

3.5. Further discussion

Water-to-binder mass ratio, and waterglass and fly ash contents, as the crucial parameters for slag-based GC, significantly influence the engineering properties including slump, and static and dynamic compressive performance. Although the previous research [20, 50–52] has investigated those influences on the different performance responses of GC, it can be learned from the current study that the influences of those parameters on the workability and mechanical response of slag-based GC are profound. On the other hand, compared with OPC-based concrete, there are more variables that affect the performance of slag-based GC. As a result, there is the complexity of mixture design and variation of the resultant performance of slag-based GC.

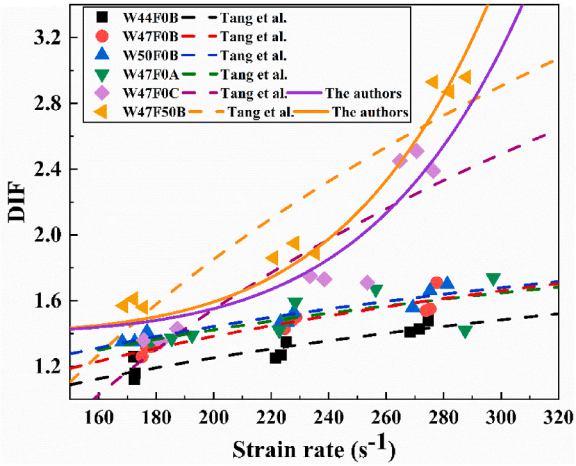

Fig. 12. Comparison of DIF between the experimental results and models proposed by Tang et al. [44] and the authors.

Table 4
Parameters of the fitting outcomes based on the model proposed by Tang et al. [44] and the authors.

Model	W44F0B	W47F0B	W50F0B	W47F0A	W47F0C	W47F50B
Tang et al. [44]						
A	1.312	1.569	1.339	1.272	5.364	5.983
B	128.41	113.90	93.29	92.94	158.12	144.10
R^2	0.882	0.885	0.886	0.852	0.758	0.833
The authors						
A	-	-	-	-	3.01×10^{-15}	2.37×10^{-15}
R^2	-	-	-	-	0.886	0.958

In this study, it can be found that there is a similarity of slag-based GC to that of OPC-based concrete. For example, the specimens with a higher static compressive strength have a higher elastic modulus, which show higher brittleness, leading to the absence of the stress-strain curve at the descending portion. The cubic compressive strengths of the specimens with 8% waterglass and 50% fly ash are both similar, while their dynamic mechanical responses are different, as shown in Figs. 10–12. Fig. 13 shows SEM images of matrices of W47F0B and W47F50B. The incorporation of fly ash appears to have a less significant influence on the homogeneity of the matrix, and the unreacted fly ash particles are observed. This demonstrates that unreacted fly ash in the matrix would play a role as fillers, which would contribute to the transferring of loading. As a consequence, a better post-peak behavior of the specimens with high amount of fly ash is obtained.

In other words, although the compressive strength has been regarded as a crucial index for guiding the structural research and design for GC [50,51,53], these variables dominate the changes of the intrinsic performance of geopolymer. Therefore, more attention

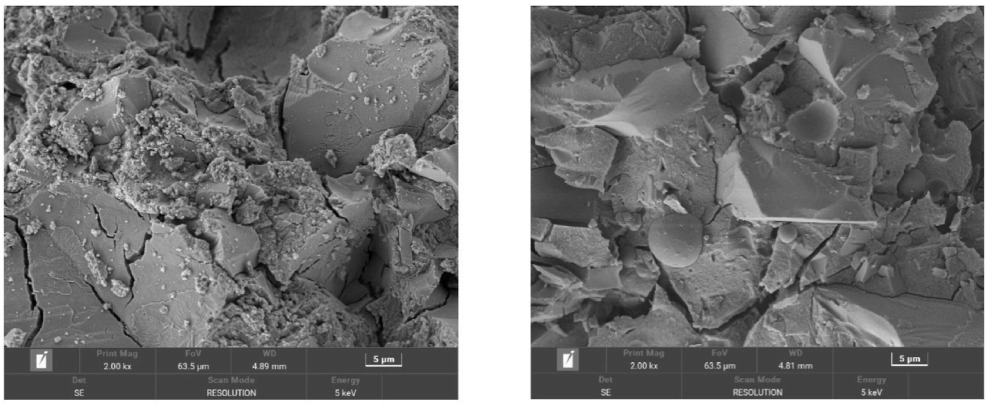

Fig. 13. SEM images of (a) W47F0B and (b) W47F50B.

should be paid to these parameters for future GC research, rather than the compressive strength grade only.

4. Conclusions

Comprehensive experimental studies were carried out to evaluated the influences of the water-to-binder mass ratio, fly ash, and waterglass contents on the slump and static and dynamic compressive behavior of slag-based GC in this study. Based on the results acquired, two empirical equations for the static and dynamic compressive stress-strain curves of slag-based GC were proposed. And the following conclusions can be drawn:

(1) The increases of water-to-binder mass ratio, and fly ash and waterglass contents contributed to the improvement of the workability of slag-based GC; nevertheless, the positive effect of waterglass content became less when the waterglass content exceeded 12%.
(2) Increasing the water-to-binder ratio resulted in the decrease of the cubic compressive strength of slag-based GC. The cubic compressive strength linearly increased as the waterglass content increased from 8% to 16%. Incorporations of fly ash led to the reduction in the cubic compressive strength.
(3) All the static compressive stress-strain curves of slag-based GC exhibited a linear ascending portion at the initial part. However, the increase of the stress became slow when the stress increased to about 80% peak stress. The mixture design parameters had a significant influence on the compressive behavior at the post-peak stage. a complete descending curve could be obtained in the specimens with lower water-to-binder ratios, higher waterglass content, and lower fly ash content. The elastic modulus and peak stress decreased as the water-to-binder mass ratio and fly ash content increased. The specimens with higher waterglass content showed a higher brittleness.
(4) The existing strain-stress models for GC did not fit the results in this study well. A new stress-strain model for slag-based GC was proposed based on the models proposed by Guo et al. and Tang et al. This model had very good outcomes for slag-based GC with different mixture design parameters.
(5) The dynamic compressive strength of all slag-based GC increased with the increase of strain rate. The increase of water-to-binder mass ratio induced the reduction in dynamic compressive strength. The increases of waterglass and fly ash contents led to higher brittleness of the specimens. Moreover, the inclusion of 50% fly ash resulted in a considerable improvement of the dynamic compressive strength at higher strain rate ($>225\ s^{-1}$).
(6) The DIFs of slag-based GC with different water-to-binder mass ratios, and waterglass and fly ash contents increased with the increase of the strain rate. However, the existing equations for predicting DIF were not satisfied with the experimental results of the specimens with higher waterglass and fly ash contents. A high-accuracy empirical formulation based on the power function was proposed in this study, as a complement of predicting DIF of the specimens of slag-based GC with higher strain-rate sensitivity.

Credit authorship contribution statement

Zhihua Ou: Conceptualization, methodology, Writing – original draft, Writing - review & editing, Funding acquisition. Ruiping Feng: Software, writing - original draft preparation. Taiwei Mao: Writing - review & editing. Ning Li: Conceptualization, Supervision, Writing - review & editing.

Declaration of competing interest

The authors declare that they have no known competing financial interests or personal relationships that could have appeared to influence the work reported in this paper.

References

[1] Y. Ding, J.-G. Dai, C.-J. Shi, Mechanical properties of alkali-activated concrete: a state-of-the-art review, Constr. Build. Mater. 127 (2016) 68–79.
[2] J. Zhang, C. Shi, Z. Zhang, Z. Ou, Durability of alkali-activated materials in aggressive environments: a review on recent studies, Constr. Build. Mater. 152 (2017) 598–613.
[3] C. Shi, B. Qu, J.L. Provis, Recent progress in low-carbon binders, Cement Concr. Res. 122 (2019) 227–250.
[4] R. Cai, H. Ye, Clinkerless ultra-high strength concrete based on alkali-activated slag at high temperatures, Cement Concr. Res. 145 (2021), 106465.
[5] Y. Liu, C. Shi, Z. Zhang, N. Li, An overview on the reuse of waste glasses in alkali-activated materials, Resour. Conserv. Recycl. 144 (2019) 297–309.
[6] L.K. Turner, F.G. Collins, Carbon dioxide equivalent (CO2-e) emissions: a comparison between geopolymer and OPC cement concrete, Constr. Build. Mater. 43 (2013) 125–130.
[7] Z. Zhang, Y. Zhu, T. Yang, L. Li, H. Zhu, H. Wang, Conversion of local industrial wastes into greener cement through geopolymer technology: a case study of high-magnesium nickel slag, J. Clean. Prod. 141 (2017) 463–471.
[8] X. Cong, W. Zhou, M. Elchalakani, Experimental study on the engineering properties of alkali-activated GGBFS/FA concrete and constitutive models for performance prediction, Constr. Build. Mater. 240 (2020), 117977.
[9] Y. Gao, J. Xu, E. Bai, X. Luo, J. Zhu, L. Nie, Static and dynamic mechanical properties of high early strength alkali activated slag concrete, Ceram. Int. 41 (10) (2015) 12901–12909. Part A).
[10] N. Li, C. Shi, Z. Zhang, H. Wang, Y. Liu, A review on mixture design methods for geopolymer concrete, Compos. B Eng. 178 (2019), 107490.
[11] Y. Liu, Z. Zhang, C. Shi, D. Zhu, N. Li, Y. Deng, Development of ultra-high performance geopolymer concrete (UHPGC): influence of steel fiber on mechanical properties, Cement Concr. Compos. 112 (2020), 103670.
[12] A. Bhutta, P.H.R. Borges, C. Zanotti, M. Farooq, N. Banthia, Flexural behavior of geopolymer composites reinforced with steel and polypropylene macro fibers, Cement Concr. Compos. 80 (2017) 31–40.
[13] A.M. Fernandez-Jimenez, A. Palomo, C. Lopez-Hombrados, Engineering properties of alkali-activated fly ash concrete, ACI Mater. J. 103(2).

[14] Y. Liu, C. Shi, Z. Zhang, N. Li, D. Shi, Mechanical and fracture properties of ultra-high performance geopolymer concrete: effects of steel fiber and silica fume, Cement Concr. Compos. 112 (2020), 103665.
[15] M. Sofi, J.S.J. van Deventer, P.A. Mendis, G.C. Lukey, Engineering properties of inorganic polymer concretes (IPCs), Cement Concr. Res. 37 (2) (2007) 251–257.
[16] L. Xin, X. Jin-yu, L. Weimin, B. Erlei, Effect of alkali-activator types on the dynamic compressive deformation behavior of geopolymer concrete, Mater. Lett. 124 (2014) 310–312.
[17] A. Karimipour, J. de Brito, Influence of polypropylene fibres and silica fume on the mechanical and fracture properties of ultra-high-performance geopolymer concrete, Constr. Build. Mater. 283 (2021), 122753.
[18] Y. Ding, C.-J. Shi, N. Li, Fracture properties of slag/fly ash-based geopolymer concrete cured in ambient temperature, Constr. Build. Mater. 190 (2018) 787–795.
[19] S. Zhang, Z. Li, B. Ghiassi, S. Yin, G. Ye, Fracture properties and microstructure formation of hardened alkali-activated slag/fly ash pastes, Cement Concr. Res. 144 (2021), 106447.
[20] N. Li, C. Shi, Z. Zhang, Understanding the roles of activators towards setting and hardening control of alkali-activated slag cement, Compos. B Eng. 171 (2019) 34–45.
[21] K.C. Reddy, C. Gudur, K.V.L. Subramaniam, Study on the influences of silica and sodium in the alkali-activation of ground granulated blast furnace slag, Constr. Build. Mater. 257 (2020), 119514.
[22] N. Li, C. Shi, Z. Zhang, D. Zhu, H.-J. Hwang, Y. Zhu, T. Sun, A mixture proportioning method for the development of performance-based alkali-activated slag-based concrete, Cement Concr. Compos. 93 (2018) 163–174.
[23] Z. Tang, Y. Hu, V.W.Y. Tam, W. Li, Uniaxial compressive behaviors of fly ash/slag-based geopolymeric concrete with recycled aggregates, Cement Concr. Compos. 104 (2019), 103375.
[24] R. Carvalho, R.V. Silva, J. de Brito, M.F.C. Pereira, Alkali activation of bottom ash from municipal solid waste incineration: optimization of NaOH- and Na 2SiO3-based activators, J. Clean. Prod. 291 (2021), 125930.
[25] P. Duxson, J.L. Provis, G.C. Lukey, S.W. Mallicoat, W.M. Kriven, J.S.J. van Deventer, Understanding the relationship between geopolymer composition, microstructure and mechanical properties, Colloids Surf., A 269 (1) (2005) 47–58.
[26] GB/T 50080-2016, Standard for Test Method of Performance on Ordinary Fresh Concrete, Chinese standard, 2017.
[27] AS 1012.3.1, Methods of Testing Concrete - Method 9: Determination of Properties Related to the Consistency of Concrete - Slump Test, Australian standard, 1998.
[28] GB/T 50081-2016: Standard of Test Methods for Mechanical Properties of Common Concrete, Chinese Standard.
[29] C. Jolicoeur, M. Simard, J. Sharman, R. Zamojska, M. Dupuis, N. Spiratos, E. Douglas, V. Malhotra, Chemical Activation of Blast-Furnace Slag, an Overview and Systematic Experimental Investigation, Advances in Concrete Technology, Ministry of Supply and Services, Canada, 1992, pp. 471–502.
[30] A. Kashani, J.L. Provis, G.G. Qiao, J.S.J. van Deventer, The interrelationship between surface chemistry and rheology in alkali activated slag paste, Constr. Build. Mater. 65 (2014) 583–591.
[31] C. Lu, Z. Zhang, C. Shi, N. Li, D. Jiao, Q. Yuan, Rheology of alkali-activated materials: a review, Cement Concr. Compos. 121 (2021), 104061.
[32] X. Dai, S. Aydın, M.Y. Yardımcı, K. Lesage, G. De Schutter, Effects of activator properties and GGBFS/FA ratio on the structural build-up and rheology of AAC, Cement Concr. Res. 138 (2020), 106253.
[33] K. Vance, A. Kumar, G. Sant, N. Neithalath, The rheological properties of ternary binders containing Portland cement, limestone, and metakaolin or fly ash, Cement Concr. Res. 52 (2013) 196–207.
[34] S.-D. Wang, K.L. Scrivener, P.L. Pratt, Factors affecting the strength of alkali-activated slag, Cement Concr. Res. 24 (6) (1994) 1033–1043.
[35] P. Nath, P.K. Sarker, Effect of GGBFS on setting, workability and early strength properties of fly ash geopolymer concrete cured in ambient condition, Constr. Build. Mater. 66 (2014) 163–171.
[36] N. Zhang, A. Hedayat, H.G. Bolaños Sosa, J.J. González Cárdenas, G.E. Salas Álvarez, V.B. Ascuña Rivera, Specimen size effects on the mechanical behaviors and failure patterns of the mine tailings-based geopolymer under uniaxial compression, Constr. Build. Mater. 281 (2021), 122525.
[37] A. Noushini, F. Aslani, A. Castel, R.I. Gilbert, B. Uy, S. Foster, Compressive stress-strain model for low-calcium fly ash-based geopolymer and heat-cured Portland cement concrete, Cement Concr. Compos. 73 (2016) 136–146.
[38] J. Němeček, V. Šmilauer, L. Kopecký, Nanoindentation characteristics of alkali-activated aluminosilicate materials, Cement Concr. Compos. 33 (2) (2011) 163–170.
[39] M.P. Collins, D. Mitchell, Prestressed Concrete Structures, Prentice Hall, Inc., Englewood Cliffs, NJ, 1991.
[40] Z. Guo, X. Zhang, D. Zhang, R. Wang, Experimental investigation of the complete stress-strain curve of concrete, J. Build. Struct. 1 (1982) 1–12.
[41] U.S. Lindholm, Some experiments with the split hopkinson pressure bar, J. Mech. Phys. Solid. 12 (5) (1964) 317–335.
[42] Z. Li, W. Chen, H. Hao, M.Z.N. Khan, T.M. Pham, Dynamic compressive properties of novel lightweight ambient-cured EPS geopolymer composite, Constr. Build. Mater. 273 (2021), 122044.
[43] Z. Wu, C. Shi, W. He, D. Wang, Static and dynamic compressive properties of ultra-high performance concrete (UHPC) with hybrid steel fiber reinforcements, Cement Concr. Compos. 79 (2017) 148–157.
[44] Z. Tang, W. Li, V.W.Y. Tam, Z. Luo, Investigation on dynamic mechanical properties of fly ash/slag-based geopolymeric recycled aggregate concrete, Compos. B Eng. 185 (2020), 107776.
[45] T.M. Pham, J. Liu, P. Tran, V.-L. Pang, F. Shi, W. Chen, H. Hao, T.M. Tran, Dynamic compressive properties of lightweight rubberized geopolymer concrete, Constr. Build. Mater. 265 (2020), 120753.
[46] X. Luo, J.-y. Xu, E.-l. Bai, W. Li, Research on the dynamic compressive test of highly fluidized geopolymer concrete, Constr. Build. Mater. 48 (2013) 166–172.
[47] K.N. Feng, D. Ruan, Z. Pan, F. Collins, Y. Bai, C.M. Wang, W.H. Duan, Mechanical behavior of geopolymer concrete subjected to high strain rate compressive loadings, Mater. Struct. 48 (3) (2015) 671–681.
[48] G. Cusatis, Strain-rate effects on concrete behavior, Int. J. Impact Eng. 38 (4) (2011) 162–170.
[49] CEB-FIB Model Code 1990. Bulletin No. 213/214, Comite International du Beton, 1993.
[50] C. Wu, H.-J. Hwang, C. Shi, N. Li, Y. Du, Shear tests on reinforced slag-based geopolymer concrete beams with transverse reinforcement, Eng. Struct. 219 (2020), 110966.
[51] Y. Du, J. Wang, C. Shi, H.-J. Hwang, N. Li, Flexural behavior of alkali-activated slag-based concrete beams, Eng. Struct. 229 (2021), 111644.
[52] N. Li, C. Shi, Q. Wang, Z. Zhang, Z. Ou, Composition design and performance of alkali-activated cements, Mater. Struct. 50 (3) (2017) 178.
[53] W. Yao, K. Xia, Y. Liu, Y. Shi, K. Peterson, Dependences of dynamic compressive and tensile strengths of four alkali-activated mortars on the loading rate and curing time, Constr. Build. Mater. 202 (2019) 891–903.